

**Effects of the Structure and Temperature on the Nature of Excitons in the  
Mo<sub>0.6</sub>W<sub>0.4</sub>S<sub>2</sub> Alloy**

Poonia, Deepika; Singh, Nisha; Schulpen, Jeff J.P.M.; Van Der Laan, Marco; Maiti, Sourav; Failla, Michele; Kinge, Sachin; Bol, Ageeth A.; Schall, Peter; Siebbeles, Laurens D.A.

**DOI**

[10.1021/acs.jpcc.1c09806](https://doi.org/10.1021/acs.jpcc.1c09806)

**Publication date**

2021

**Document Version**

Final published version

**Published in**

Journal of Physical Chemistry C

**Citation (APA)**

Poonia, D., Singh, N., Schulpen, J. J. P. M., Van Der Laan, M., Maiti, S., Failla, M., Kinge, S., Bol, A. A., Schall, P., & Siebbeles, L. D. A. (2021). Effects of the Structure and Temperature on the Nature of Excitons in the Mo<sub>0.6</sub>W<sub>0.4</sub>S<sub>2</sub> Alloy. *Journal of Physical Chemistry C*, 126(4), 1931-1938. <https://doi.org/10.1021/acs.jpcc.1c09806>

**Important note**

To cite this publication, please use the final published version (if applicable).  
Please check the document version above.

**Copyright**

Other than for strictly personal use, it is not permitted to download, forward or distribute the text or part of it, without the consent of the author(s) and/or copyright holder(s), unless the work is under an open content license such as Creative Commons.

**Takedown policy**

Please contact us and provide details if you believe this document breaches copyrights.  
We will remove access to the work immediately and investigate your claim.

# Effects of the Structure and Temperature on the Nature of Excitons in the $\text{Mo}_{0.6}\text{W}_{0.4}\text{S}_2$ Alloy

Deepika Poonia,<sup>†</sup> Nisha Singh,<sup>†</sup> Jeff J. P. M. Schulpen, Marco van der Laan, Sourav Maiti, Michele Failla, Sachin Kinge, Ageeth A. Bol, Peter Schall, and Laurens D. A. Siebbeles\*



Cite This: *J. Phys. Chem. C* 2022, 126, 1931–1938



Read Online

ACCESS |



Metrics & More

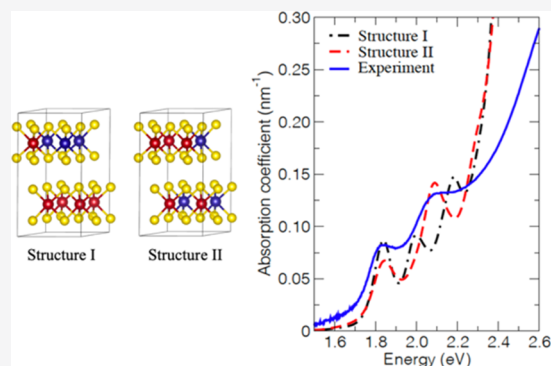


Article Recommendations



Supporting Information

**ABSTRACT:** We studied the nature of excitons in the transition metal dichalcogenide alloy  $\text{Mo}_{0.6}\text{W}_{0.4}\text{S}_2$  compared to pure  $\text{MoS}_2$  and  $\text{WS}_2$  grown by atomic layer deposition (ALD). For this, optical absorption/transmission spectroscopy and time-dependent density functional theory (TDDFT) were used. The effects of temperature on A and B exciton peak energies and line widths in optical transmission spectra were compared between the alloy and pure  $\text{MoS}_2$  and  $\text{WS}_2$ . On increasing the temperature from 25 to 293 K, the energy of the A and B exciton peaks decreases, while their line width increases due to exciton–phonon interactions. The exciton–phonon interactions in the alloy are closer to those for  $\text{MoS}_2$  than those for  $\text{WS}_2$ . This suggests that exciton wave functions in the alloy have a larger amplitude on Mo atoms than that on W atoms. The experimental absorption spectra could be reproduced by TDDFT calculations. Interestingly, for the alloy, the Mo and W atoms had to be distributed over all layers. Conversely, we could not reproduce the experimental alloy spectrum by calculations on a structure with alternating layers, in which every other layer contains only Mo atoms and the layers in between also contain W atoms. For the latter atomic arrangement, the TDDFT calculations yielded an additional optical absorption peak that could be due to excitons with some charge transfer character. From these results, we conclude that ALD yields an alloy in which Mo and W atoms are distributed uniformly among all layers.



## 1. INTRODUCTION

Layered van der Waals materials, in particular transition metal dichalcogenides (TMDCs), have gained considerable interest due to prospects for applications in, e.g., photodetectors,<sup>1,2</sup> sensors,<sup>3,4</sup> and solar cells.<sup>5–7</sup> These materials consist of layers in which transition metal atoms are covalently bound to chalcogen (S, Se, Te) atoms. The layers are stacked on top of each other and held together by van der Waals forces.<sup>8,9</sup> TMDCs with chemical composition  $\text{MX}_2$  ( $M = \text{Mo}, \text{W}$ , etc., and  $X = \text{S}, \text{Se}$ ) have been studied extensively owing to their direct band gap in monolayers,<sup>10</sup> valley selective optical coupling,<sup>11</sup> and large exciton binding energies.<sup>12</sup> Alloying has been used to vary the relative content ( $y$ ) of the transition metal or chalcogen atoms and obtain layers of  $\text{M}_y\text{M}'_{1-y}\text{X}_2$  or  $\text{MX}_2\text{X}'_{2(1-y)}$ .<sup>13,14</sup> For monolayers of  $\text{Mo}_y\text{W}_{1-y}\text{S}_2$  alloys, it was found that the Mo and W atoms are spatially distributed in a random way.<sup>15</sup> Increasing the W content in samples of one or a few  $\text{Mo}_y\text{W}_{1-y}\text{S}_2$  layers caused a blue shift of the exciton peak in optical absorption and reflection spectra,<sup>16,17</sup> in agreement with time-dependent density functional theory (TDDFT) calculations.<sup>18</sup> According to DFT calculations, the valence band of monolayer  $\text{Mo}_{0.5}\text{W}_{0.5}\text{S}_2$  consists of atomic d-orbitals on both Mo and W atoms, while the conduction band consists predominantly of d-orbitals on Mo atoms.<sup>19</sup>

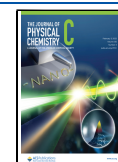
For optoelectronic applications, an understanding of electron–phonon and exciton–phonon interactions is important. The strength of these interactions governs charge transport,<sup>20</sup> band gap renormalization,<sup>21</sup> optical heating of the lattice,<sup>22</sup> and intervalley scattering of excitons.<sup>23–25</sup> In this regard, effects of temperature on optical absorption and photoluminescence spectra can provide information about the coupling strength between excitons and phonons in TMDCs.<sup>23–26</sup>

More than two decades ago, Ho et al.<sup>27</sup> studied the effects of temperature on excitons in single crystals of  $\text{Mo}_y\text{W}_{1-y}\text{S}_2$  alloys by piezoreflectance measurements, which preferentially probe excitons near the sample surface. We extend these studies on the atomic layer deposited (ALD)<sup>28</sup> bulk part of the  $\text{Mo}_{0.6}\text{W}_{0.4}\text{S}_2$  alloy to investigate the effects of temperature on peak energies and line widths of excitons. The almost equal content of Mo and W atoms in the alloy is of interest since it

**Received:** November 15, 2021

**Revised:** January 13, 2022

**Published:** January 25, 2022



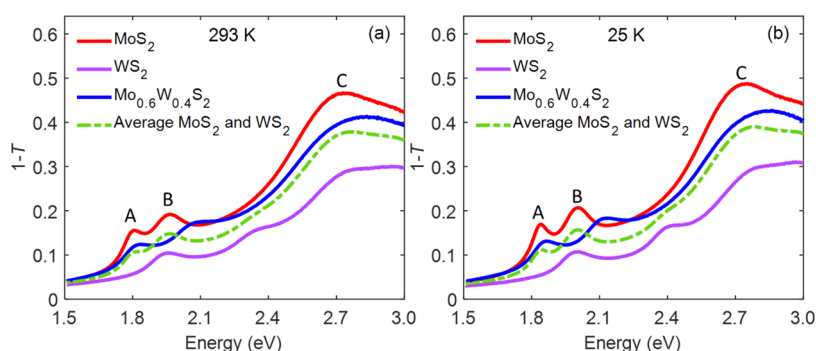


**Figure 1.** (a) Room-temperature (293 K) and (b) low-temperature (25 K) optical transmission spectra of MoS<sub>2</sub> (red), WS<sub>2</sub> (magenta), and the Mo<sub>0.6</sub>W<sub>0.4</sub>S<sub>2</sub> alloy (blue). The dashed green curves are the average of the MoS<sub>2</sub> and WS<sub>2</sub> spectra.

offers the possibility to realize intimate mixing of the transition metal atoms rather than having separate domains consisting of one atom type only. To elucidate the effects of the relative arrangement of Mo and W atoms in the alloy, we compared the measured spectra with results from *ab initio* TDDFT calculations. For this purpose, we constructed supercells having different positions of the metal atoms in the crystal structure of the alloy. The TDDFT calculations reproduced the experimental spectrum of the alloy for structures in which all layers contain both Mo and W atoms. In contrast, calculations on a structure containing W atoms in individual layers that are separated by layers containing only Mo atoms do not reproduce the experimental spectrum. From the latter, we infer that the ALD growth yields structures with a predominantly homogeneous spatial distribution of Mo and W atoms.

## 2. METHODS

**2.1. Temperature-Dependent Optical Transmission Measurements.** We used our previously reported ALD procedure to grow thin films of MoS<sub>2</sub>, WS<sub>2</sub>, and the Mo<sub>0.6</sub>W<sub>0.4</sub>S<sub>2</sub> alloy, with thicknesses of 6.3, 4.1, and 5.2 nm, respectively, on quartz substrates.<sup>28</sup> The uncertainty in the fraction of Mo and W is  $\pm 0.01$ .<sup>28</sup> The alloy was grown using an ALD supercycle length of two cycles (consisting of one MoS<sub>2</sub> cycle and one WS<sub>2</sub> cycle), to realize fine mixing of the Mo and W atoms. The composition was determined by X-ray photoelectron spectroscopy (XPS).<sup>28</sup> The separation between adjacent layers in these materials is  $\sim 0.6$  nm, so the film thicknesses correspond to 10–11, 6–7, and 8–9 layers, respectively.

The optical transmission of the samples was measured using a home-built setup containing a DH-2000 halogen light source and an Ocean-optics Maya 2000 spectrometer. To vary the temperature, the samples were placed under vacuum in a He-closed cycle cryostat. These measurements yield the fraction of light transmitted,  $T$ , through the sample as a function of photon energy and temperature.

For the comparison of the optical properties of the samples with the optical absorption coefficient from TDDFT calculations (see Section 3.3), we determined the optical density (OD), using a PerkinElmer Lambda 1050 spectrometer with an integrating sphere. This could be done only at room temperature since the spectrometer was not equipped with a cryostat. Placing the sample in front of the light entrance of the integrating sphere yielded  $T$ , and placing it in the center provided  $T + R$ , where  $R$  is the fraction of light reflected. The

results of  $1 - T$ ,  $R$ , and the fraction of light absorbed  $A = 1 - R - T$  are shown in Figure S1 for the pure compounds and the alloy. The optical density was obtained using the relation  $OD = -\log\left(\frac{T}{1-R}\right)$ . The optical absorption coefficient,  $\alpha$ , of a film with thickness  $L$  is related to the OD according to  $e^{-\alpha L} = 10^{-OD}$ , giving  $\alpha = OD \ln(10)/L$ .

**2.2. TDDFT Calculations of Optical Absorption Coefficients.** Electronic structure calculations were performed using the all-electron full-potential linearized augmented plane wave (LAPW) code Elk<sup>29</sup> with PBE (GGA) functionals.<sup>30</sup> For all materials, a hexagonal crystal structure (2H) was used, with experimental lattice constants of 3.169 and 12.324 Å for MoS<sub>2</sub><sup>31</sup> and 3.153 and 12.323 Å for WS<sub>2</sub>.<sup>32</sup> A  $2 \times 2 \times 1$  supercell was constructed to study the Mo<sub>0.625</sub>W<sub>0.375</sub>S<sub>2</sub> alloy with lattice parameters of 6.338 and 12.324 Å obtained by doubling the MoS<sub>2</sub> unit cell. This is the smallest supercell describing the experimentally studied alloy with a composition very close to the experimental uncertainty (see Section 2.1). Note that larger supercells can be constructed. However, we only considered the  $2 \times 2 \times 1$  supercell because larger supercells require significantly more computational time (at least 1 order of magnitude) and more computer memory. The calculation of the dielectric response functions from TDDFT required a dense  $k$ -point grid to sample the Brillouin zone (BZ), hence a  $k$ -point grid of  $16 \times 16 \times 8$  for the primitive unit cell and an  $8 \times 8 \times 8$   $k$ -point grid for the supercell were used. The set of LAPW basis functions was defined by specifying a cutoff parameter  $|k + G|_{\max}$  whose value was set to 7.0 Bohr<sup>-1</sup>. Additionally, the response was calculated using  $G$  vectors of 1.5 Bohr<sup>-1</sup> length. The number of conduction bands included in the calculations was 24 for both MoS<sub>2</sub> and WS<sub>2</sub> and 96 for the alloy.

In TDDFT, a Dyson-like equation was solved to obtain the dielectric response function<sup>33</sup> whose real and imaginary parts can be used to obtain the optical absorption coefficient  $\alpha$ .<sup>34</sup> The method to obtain optical response functions was a two-step procedure. First, a ground-state calculation was done to obtain the converged density and potentials. Next, the dielectric functions of MoS<sub>2</sub>, WS<sub>2</sub>, and the Mo<sub>0.625</sub>W<sub>0.375</sub>S<sub>2</sub> alloy were calculated as a function of photon energy using the bootstrap kernel,<sup>35</sup> as it was capable of capturing excitons in the TDDFT calculations. The dielectric functions thus obtained were broadened by 80 meV for MoS<sub>2</sub> and WS<sub>2</sub> and 54 meV for the alloy to obtain the best matches with the experimental optical absorption coefficient spectra ( $\alpha$ ). Note that the broadening thus introduced in the calculated spectra

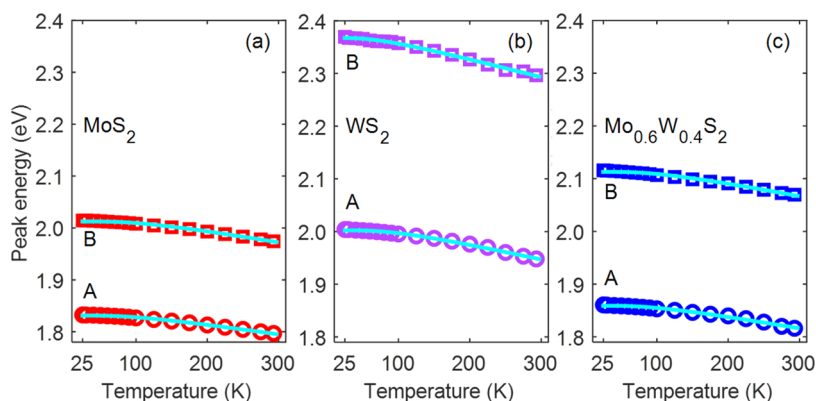


**Figure 2.** Temperature dependence of the A and B exciton peak energies for (a) MoS<sub>2</sub>, (b) WS<sub>2</sub>, and (c) the Mo<sub>0.6</sub>W<sub>0.4</sub>S<sub>2</sub> alloy, obtained from the measured transmission spectra (markers). The solid cyan curves are fits of eq 1 to the experimental peak energies.

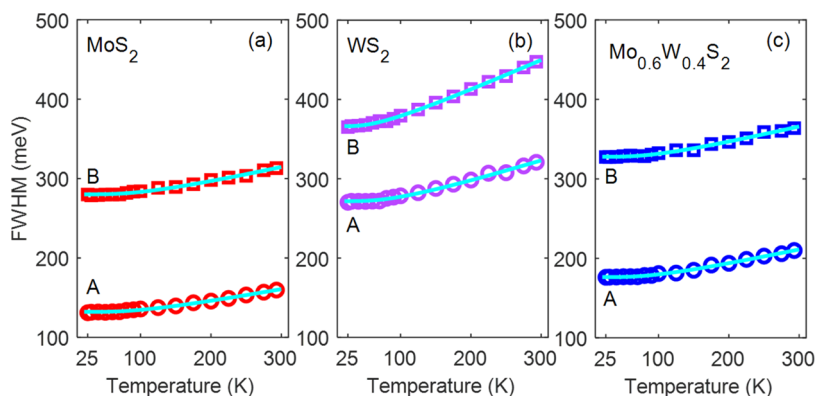


**Figure 3.** Temperature dependence of the line widths (FWHM, markers) of the A and B exciton peaks for (a) MoS<sub>2</sub>, (b) WS<sub>2</sub>, and (c) the Mo<sub>0.6</sub>W<sub>0.4</sub>S<sub>2</sub> alloy. The solid cyan lines are fits to the experimental data.

did not explain the exciton line widths in the experimental spectra.

The absolute values of exciton energies with respect to the ground state cannot be accurately captured by TDDFT, due to the well-known band gap problem. To overcome this, we employed the so-called “scissor operator” method that shifts the entire optical absorption spectrum ( $\alpha$ ) in energy. To reproduce the lowest experimental exciton energy, we used energy shifts of 0.03, 0.08, and 0.06 eV for MoS<sub>2</sub>, WS<sub>2</sub>, and the Mo<sub>0.625</sub>W<sub>0.375</sub>S<sub>2</sub> alloy, respectively.

### 3. RESULTS AND DISCUSSION

**3.1. Optical Transmission Spectra.** Figure 1a shows the optical transmission spectra of MoS<sub>2</sub>, WS<sub>2</sub>, and the Mo<sub>0.6</sub>W<sub>0.4</sub>S<sub>2</sub> alloy at room temperature (293 K). These spectra show the magnitude of  $1 - T$ , which is the fraction of incident light that is not transmitted through the sample. The spectra of MoS<sub>2</sub> and WS<sub>2</sub> agree with previous results.<sup>8,36</sup> Two distinct peaks (marked by A and B) can be seen in all three materials. The peaks are due to photoexcitation from the ground state to A and B exciton states. The energies of these peaks are determined by spin–orbit coupling and interlayer interactions at the  $K$  and  $K'$  points of the Brillouin zone (BZ).<sup>37–39</sup> Toward the higher energy side, a broad absorption feature is observed (often addressed as C exciton), which originates from multiple transitions from the highest valence band to the lowest conduction bands near the  $\Gamma$  point of the BZ.<sup>40</sup> On lowering the temperature to 25 K (Figure 1b), the exciton peaks of all three materials become narrower and shift to higher energy.

**Table 1.** Fitted Values of the Exciton–Phonon Coupling Strength,  $S_X$ , the Average Phonon Energy,  $\langle \hbar\omega_X \rangle$ , Inhomogeneous Line Width Broadening,  $\Gamma_{X,l}$ , and the Exciton–Phonon Interaction Strength,  $\Gamma_{X,ph}$ , for MoS<sub>2</sub>, WS<sub>2</sub>, and the Mo<sub>0.6</sub>W<sub>0.4</sub>S<sub>2</sub> Alloy

	MoS <sub>2</sub>	WS <sub>2</sub>	Mo <sub>0.6</sub> W <sub>0.4</sub> S <sub>2</sub>
$E_{0A}$ (eV)	$1.80 \pm 0.01$	$1.96 \pm 0.01$	$1.83 \pm 0.01$
$E_{0B}$ (eV)	$1.97 \pm 0.01$	$2.34 \pm 0.01$	$2.09 \pm 0.01$
$S_A$	$1.4 \pm 0.2$	$1.9 \pm 0.2$	$1.5 \pm 0.1$
$S_B$	$1.5 \pm 0.1$	$2.1 \pm 0.1$	$1.6 \pm 0.1$
$\hbar\omega_A$ (meV)	$26.4 \pm 2.2$	$22.8 \pm 3.1$	$24.4 \pm 2.5$
$\hbar\omega_B$ (meV)	$26.4 \pm 1.9$	$16.4 \pm 3.5$	$24.4 \pm 1.5$
$\Gamma_{A,l}$ (meV)	$132.1 \pm 0.4$	$271.8 \pm 0.9$	$176.4 \pm 0.1$
$\Gamma_{B,l}$ (meV)	$280.2 \pm 0.7$	$366.2 \pm 0.6$	$327.8 \pm 0.1$
$\Gamma_{A,ph}$ (meV)	$50.8 \pm 1.8$	$72.4 \pm 3.0$	$54.6 \pm 1.9$
$\Gamma_{B,ph}$ (meV)	$60.8 \pm 3.1$	$73.9 \pm 1.6$	$59.7 \pm 2.5$

To gain qualitative insights into the effect of alloying, we also show the average of the spectra of pure MoS<sub>2</sub> and WS<sub>2</sub> as green dashed curves in Figure 1 (a quantitative comparison of the measured OD and the results from TDDFT is discussed in Section 3.3). The average spectra at 293 and 25 K both differ from the spectra of the alloy. Most strikingly, the B exciton peak of the alloy appears at significantly higher energy than in the average spectra. These differences indicate that formation of excitons in domains consisting of either predominantly MoS<sub>2</sub> or WS<sub>2</sub> is unlikely. As a consequence, the probability that photoexcitation leads to formation of a charge transfer



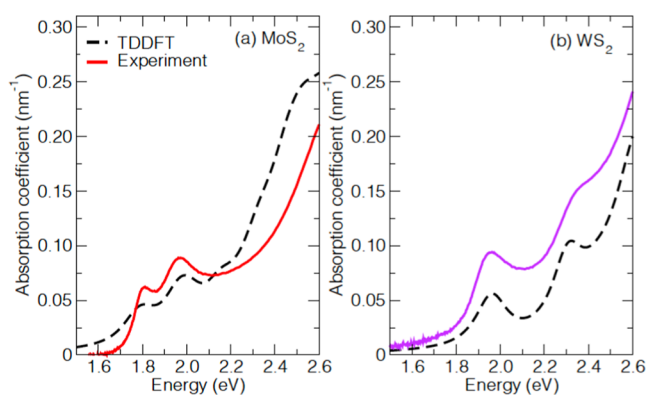


**Figure 4.** Absorption coefficient,  $\alpha$ , obtained from TDDFT calculations (black dashed curves) together with the experimental results at 293 K for (a) MoS<sub>2</sub> and (b) WS<sub>2</sub>.

**Table 2.** Energies of the A and B Excitons in MoS<sub>2</sub>, WS<sub>2</sub>, and the Mo<sub>0.6</sub>W<sub>0.4</sub>S<sub>2</sub> Alloy<sup>a</sup>

	MoS <sub>2</sub>	WS <sub>2</sub>	Mo <sub>0.6</sub> W <sub>0.4</sub> S <sub>2</sub>	Mo <sub>0.625</sub> W <sub>0.375</sub> S <sub>2</sub>
$E_A$ (exp.) (eV)	1.80	1.96	1.83	
$E_B$ (exp.) (eV)	1.97	2.34	2.09	
$E_B - E_A$ (exp.) (meV)	170	380	260	
$E_B - E_A$ (TDDFT calc.) (meV)	179	353		255

<sup>a</sup>The last two rows show the energy difference between the exciton energies from experiments (exp.) and the TDDFT calculations.

exciton at a boundary between these material domains is small. Indeed, the peak of the A exciton in the alloy spectrum appears at higher energy than that in the spectrum of MoS<sub>2</sub>, while that of a charge transfer exciton would be at lower energy.

Inspection of the transmission spectra of the alloy points toward closer similarities to MoS<sub>2</sub> than to WS<sub>2</sub>. Despite intimate mixing and nearly equal Mo and W content in the alloy,<sup>28</sup> the energies of the A and B excitons in the alloy are closer to those of pure MoS<sub>2</sub>, as also found for samples of one or a few Mo<sub>0.5</sub>W<sub>0.5</sub>S<sub>2</sub> layers before.<sup>16,17</sup> This suggests that the wave functions of excitons in the Mo<sub>0.6</sub>W<sub>0.4</sub>S<sub>2</sub> alloy have a larger amplitude on Mo atoms than that on W atoms. The latter agrees with charge density distributions for the highest valence and lowest conduction band states obtained from DFT calculations.<sup>14,19</sup> Interestingly, according to our TDDFT calculations, the mutual arrangement of Mo and W atoms within the material has a large impact on the shape of the optical absorption spectrum (see Section 3.3). To gain insights into the nature of exciton–phonon coupling, we first proceed

with a discussion of the measured effects of temperature on exciton peak positions and line widths in Section 3.2.

**3.2. Temperature Dependence of A and B Exciton Peak Energies and Line Widths.** To gain further insights into the relative contributions of Mo and W atoms to the character of excitons, we compare the effects of exciton–phonon coupling in the Mo<sub>0.6</sub>W<sub>0.4</sub>S<sub>2</sub> alloy with those in MoS<sub>2</sub> and WS<sub>2</sub>. We studied exciton–phonon coupling by the analysis of the temperature dependence of exciton peak energies and line widths in the transmission spectra, as outlined in Section 2 in the Supporting Information. The peaks due to A and B excitons could each be described by a Lorentzian function with line width  $\Gamma_X$  (where  $X = A, B$ ), which is defined as the full width at half-maximum (FWHM), see eq S1. The contribution of optical reflection, below band gap absorption due to defects,<sup>41</sup> and the broad C absorption feature at higher energy in the optical transmission spectra in Figure 1 could be described by two Gaussian functions. The total fit function thus consists of two Lorentzian and two Gaussian functions, see eq S1. Figure S2 shows that the fits reproduce the experimental transmission spectra very well.

Figures 2 and 3 show the temperature dependence of the A and B exciton peak energies and line widths, as obtained from fits of eq S1 to the experimental transmission spectra. At all temperatures, the peak energies and line widths of the Mo<sub>0.6</sub>W<sub>0.4</sub>S<sub>2</sub> alloy are closer to those of MoS<sub>2</sub> than those of WS<sub>2</sub>. This further supports the idea that excitons have more Mo than W character, as we already inferred above from Figure 1.

The decrease of the exciton peak energies with increasing temperature is due to the availability of more phonons at higher temperatures that can be absorbed upon photoexcitation from the electronic ground state to an exciton state, as well as electron–phonon coupling due to interaction between the motion of electrons and atomic nuclei (change of bond lengths and breakdown of the Born–Oppenheimer approximation).<sup>42–44</sup> Following previous studies,<sup>26,44–46</sup> we describe the temperature dependence of the exciton peak energies by the following semiempirical O’Donnell equation<sup>47</sup>

$$E_X = E_{0,X} - S_X \langle \hbar \omega_X \rangle \left[ \coth \left( \frac{\langle \hbar \omega_X \rangle}{2k_B T} \right) - 1 \right] \quad (1)$$

where  $X = A, B$  denotes the exciton type, and  $k_B$  and  $\hbar$  are the Boltzmann and the reduced Planck constant, respectively. In eq 1,  $E_{0,X}$  is the exciton peak energy at zero temperature,  $S_X$  is a dimensionless constant that increases with the exciton–

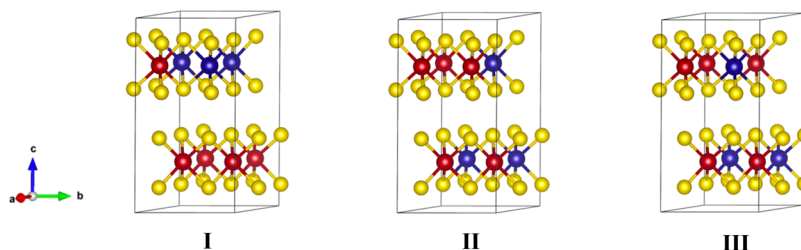


**Figure 5.** Three physically distinct arrangements of atoms in the Mo<sub>0.625</sub>W<sub>0.375</sub>S<sub>2</sub> alloy. Each 2 × 2 × 1 supercell of the Mo<sub>0.625</sub>W<sub>0.375</sub>S<sub>2</sub> alloy shows the different arrangements of metal and chalcogen atoms where the Mo atoms are red, the W atoms are blue, and the S atoms are yellow. Heterogeneous structure I has alternating layers of Mo atoms only and layers containing both Mo and W atoms. In homogeneous structures II and III, all layers contain Mo and W atoms.

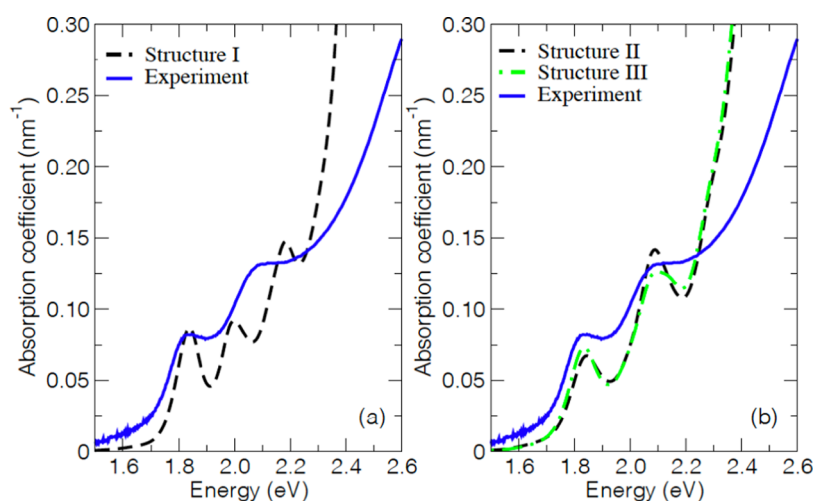


**Figure 6.** Calculated absorption coefficient of (a) structure I and (b) structures II and III of the Mo<sub>0.625</sub>W<sub>0.375</sub>S<sub>2</sub> alloy, together with the experimental spectrum at room temperature (293 K).

phonon coupling strength, and  $\langle \hbar\omega_x \rangle$  is the coupling-weighted average of the phonon energies that interact with the exciton.<sup>48</sup>

Fits of eq 1 to the A and B exciton peak energies with  $E_{0,x}$ ,  $S_x$ , and  $\langle \hbar\omega_x \rangle$  as adjustable parameters are shown as solid cyan curves in Figure 2. Equation 1 reproduces the temperature dependence of the exciton peak energies very well and the values of the fit parameters are presented in Table 1. The exciton peak energies  $E_{0,A}$  and  $E_{0,B}$  for the alloy are closer to those for MoS<sub>2</sub> than for WS<sub>2</sub>. In addition, the fitted values of  $S_A$  and  $S_B$  (near 1.5) for the alloy are similar to those of MoS<sub>2</sub>, while they are about 25% smaller than the values obtained for WS<sub>2</sub> (near 2.0). These findings corroborate our notice in Section 3.1 that exciton wave functions in the alloy have a larger amplitude on Mo atoms than that on W atoms so that the former has a predominant effect on exciton–phonon coupling. Within the experimental uncertainty, the average phonon energies  $\langle \hbar\omega_x \rangle$  for both A and B excitons are similar for all three materials and are close to the value of 22.1 meV reported for MoS<sub>2</sub> and WS<sub>2</sub> in the literature.<sup>49,50</sup>

We analyze the temperature dependence of the line widths of the Lorentzians in eq S1 of the A and B exciton peaks by using the following expression<sup>51</sup>

$$\Gamma_X = \Gamma_{X,I} + \frac{\Gamma_{X,\text{ph}}}{e^{\left(\frac{\hbar\omega_X}{k_B T}\right)} - 1} \quad (2)$$

The first term at the right-hand side of eq 2,  $\Gamma_{X,I}$ , represents inhomogeneous line width broadening induced by temperature-independent mechanisms, such as scattering of excitons on structural defects or impurities. The second term describes exciton–phonon scattering for both absorption and emission of phonons. The average energies of phonons that couple with excitons,  $\langle \hbar\omega_x \rangle$ , were taken equal to the values obtained from fitting eq 1 to the peak energies, see Table 1.

The solid cyan lines in Figure 3a–c are the least-squares fits of eq 2 to the FWHM values, with the latter obtained from fits of eq S1 to the optical transmission spectra in Figure S2. The results for the inhomogeneous broadening,  $\Gamma_{X,I}$ , and the broadening due to exciton–phonon scattering,  $\Gamma_{X,\text{ph}}$ , are presented in Table 1. For each of the three materials, the values of the inhomogeneous broadening of the A exciton,  $\Gamma_{A,I}$ , are smaller than those of the B exciton,  $\Gamma_{B,I}$ , similar to results for single crystals.<sup>52</sup> Interestingly, the values of both  $\Gamma_{A,\text{ph}}$  and

$\Gamma_{B,\text{ph}}$  of the alloy are close to the corresponding values for MoS<sub>2</sub>, while they are significantly lower than those for WS<sub>2</sub>. This is in line with the exciton peak energies and the values of  $S_A$  and  $S_B$  for the alloy being nearest to those of MoS<sub>2</sub>, as discussed above. The larger exciton–phonon scattering rate for B excitons can be due to the additional ultrafast decay channel of B excitons involving their relaxation to A excitons by emission of phonons, as discussed previously.<sup>53</sup>

Our values of  $E_{0,x}$ ,  $S_x$ ,  $\langle \hbar\omega_x \rangle$ , and  $\Gamma_{X,\text{ph}}$  for ALD-grown MoS<sub>2</sub> and WS<sub>2</sub> films are within the range reported for mono- or few-layer TMDC samples that were obtained by mechanical exfoliation or chemical vapor deposition (CVD)<sup>26,45,46,50,54–56</sup> and CVD-grown bulk samples.<sup>27,50</sup> Note that the values of these parameters can vary from one sample to another due to differences in sample preparation, dielectric environment (in particular for mono- and few-layer samples), etc. Our values for the inhomogeneous line width broadening,  $\Gamma_{X,I}$ , are higher than those that Ho et al.<sup>27</sup> obtained from temperature-dependent piezoreflectance measurements on CVD-grown crystals of MoS<sub>2</sub>, WS<sub>2</sub>, and Mo<sub>x</sub>W<sub>1-x</sub>S<sub>2</sub> alloys. This may result from a larger degree of structural disorder in our ALD-grown samples. Indeed the grain size in ALD-grown samples is  $\sim 10$  nm, which is much smaller than that for CVD-grown crystals.<sup>57</sup> Interestingly, the values of the exciton–LO phonon coupling strength,  $\Gamma_{X,\text{ph}}$ , reported by Ho et al.<sup>27</sup> are a factor of 2–3 higher than ours. This could be due to the fact that their piezoreflectance measurements probe excitons near the sample surface, which would then appear to couple to surface phonons with higher strength than the bulk exciton–phonon coupling probed in our experiments.

**3.3. TDDFT Calculations of the Optical Absorption Spectrum.** The real and imaginary parts of the dielectric functions obtained from the TDDFT calculations are shown in Figures S3–S5 and these were used to calculate the optical absorption coefficient,  $\alpha$ , according to eq S3. The calculated absorption coefficients for MoS<sub>2</sub> and WS<sub>2</sub> are shown in Figure 4, together with the experimental data at 293 K. The optical absorption coefficients were obtained, as described in Section 2.2, using the spectra of  $T$  and  $R$  in Figure S1. The calculations reproduce the relative energies of the A and B excitons very well, see also Table 2. In addition, the calculations reproduce the magnitude of the optical absorption coefficient to within a factor 2.

As discussed in Section 2, we describe the  $\text{Mo}_{0.6}\text{W}_{0.4}\text{S}_2$  alloy by a periodic crystal structure with the smallest possible ( $2 \times 2 \times 1$ ) supercell, resulting in the  $\text{Mo}_{0.625}\text{W}_{0.375}\text{S}_2$  alloy, see Figure 5. One unit cell then contains 5 Mo atoms, 3 W atoms, and 16 S atoms that are arranged in two layers bonded by van der Waals forces. By permutation of the 5 Mo and 3 W atoms, one can realize 28 different arrangements. These can be categorized into two groups: (1) 4 “heterogeneous” structures in which every other layer contains only Mo atoms and the layers in between contain also W atoms, and (2) 24 “homogeneous” structures in which both layers contain Mo and W atoms. Applying the symmetry operations of translation, rotation, mirror planes, and their combinations, we obtain three physically distinct structures (I, II, and III), as shown in Figure 5.

The calculated optical absorption coefficient of the  $\text{Mo}_{0.625}\text{W}_{0.375}\text{S}_2$  alloy with heterogeneous structure I is shown in Figure 6a, together with the experimental spectrum. The presence of three peaks in the calculated spectrum disagrees with the two excitonic peaks in the experimental spectrum. We suspect, but cannot prove here, that the peak at the lowest energy calculated for structure I is due to excitons having some more charge transfer character than the peaks at higher energy. For such excitons, the electron would have a somewhat larger probability to reside on Mo atoms, while the hole is preferentially present on W atoms. Interestingly, the calculated spectra of structures II and III shown in Figure 6b agree with the experimental spectrum. The relative energies of the A and B excitons, as well as the magnitude of the optical absorption coefficient, are very well reproduced by these structures (see Table 2). From this, we infer that the Mo and W atoms in the ALD-grown films are to a large extent mixed homogeneously, as in structures II and III. This agrees with the previously reported random arrangement of Mo and W atoms in monolayers of these alloys grown by chemical vapor transport.<sup>14,15</sup> The very different result from TDDFT calculations for structure I in Figure 6a compared with those for structures II and III in Figure 6b shows that the mutual arrangement of Mo and W atoms has a strong effect on the optical absorption spectrum.

Unfortunately, the TDDFT calculations performed with the Elk code do not provide the atom resolved composition of the exciton wave functions, and therefore, we cannot obtain the distribution of the electron and hole within an exciton among the atoms. To investigate the spatial distribution of the electron and the hole within an exciton, calculations at a higher level of theory are needed, e.g., by describing excitons on the basis of the Bethe–Salpeter equation.<sup>58</sup>

#### 4. CONCLUSIONS

We performed a combined experimental and time-dependent density functional theory (TDDFT) study of the optical absorption/transmission spectra of ALD-grown thin films of  $\text{MoS}_2$ ,  $\text{WS}_2$ , and the  $\text{Mo}_{0.6}\text{W}_{0.4}\text{S}_2$  alloy. The temperature dependence of the peak energies and line widths of the A and B excitons in the alloy is close to that for  $\text{MoS}_2$ . This suggests that the exciton wave functions have a larger amplitude on Mo atoms than that on W atoms. From the comparison of the measured optical absorption spectra with those from TDDFT calculations, we infer that Mo and W atoms are homogeneously distributed throughout the alloy. Further, the mutual arrangement of Mo and W atoms in the material has a strong effect on the shape of the optical absorption spectrum. These

results provide clear support toward structural engineering of two-dimensional van der Waals materials through atomic arrangements, extending the already rich variety of properties in this class of materials.

#### ■ ASSOCIATED CONTENT

##### Supporting Information

The Supporting Information is available free of charge at <https://pubs.acs.org/doi/10.1021/acs.jpcc.1c09806>.

Absorption spectra; fits to temperature-dependent optical transmission spectra of  $\text{MoS}_2$ ,  $\text{WS}_2$ , and the  $\text{Mo}_{0.6}\text{W}_{0.4}\text{S}_2$  alloy; and relation between absorption coefficient and dielectric function (PDF)

#### ■ AUTHOR INFORMATION

##### Corresponding Author

Laurens D. A. Siebbeles – *Optoelectronic Materials Section, Department of Chemical Engineering, Delft University of Technology, 2629 HZ Delft, The Netherlands*; [orcid.org/0000-0002-4812-7495](https://orcid.org/0000-0002-4812-7495); Email: [L.D.A.Siebbeles@tudelft.nl](mailto:L.D.A.Siebbeles@tudelft.nl)

##### Authors

Deepika Poonia – *Optoelectronic Materials Section, Department of Chemical Engineering, Delft University of Technology, 2629 HZ Delft, The Netherlands*

Nisha Singh – *Optoelectronic Materials Section, Department of Chemical Engineering, Delft University of Technology, 2629 HZ Delft, The Netherlands*; [orcid.org/0000-0002-2012-9974](https://orcid.org/0000-0002-2012-9974)

Jeff J. P. M. Schulpen – *Department of Applied Physics, Eindhoven University of Technology, 5600 MB Eindhoven, The Netherlands*

Marco van der Laan – *Institute of Physics, University of Amsterdam, 1098 XH Amsterdam, The Netherlands*; [orcid.org/0000-0001-9571-3190](https://orcid.org/0000-0001-9571-3190)

Sourav Maiti – *Optoelectronic Materials Section, Department of Chemical Engineering, Delft University of Technology, 2629 HZ Delft, The Netherlands*; [orcid.org/0000-0003-1983-9159](https://orcid.org/0000-0003-1983-9159)

Michele Failla – *Optoelectronic Materials Section, Department of Chemical Engineering, Delft University of Technology, 2629 HZ Delft, The Netherlands*; [orcid.org/0000-0001-5822-8049](https://orcid.org/0000-0001-5822-8049)

Sachin Kinge – *Materials Research & Development, Toyota Motor Europe, B1930 Zaventem, Belgium*

Ageeth A. Bol – *Department of Applied Physics, Eindhoven University of Technology, 5600 MB Eindhoven, The Netherlands*; [orcid.org/0000-0002-1259-6265](https://orcid.org/0000-0002-1259-6265)

Peter Schall – *Institute of Physics, University of Amsterdam, 1098 XH Amsterdam, The Netherlands*

Complete contact information is available at: <https://pubs.acs.org/doi/10.1021/acs.jpcc.1c09806>

##### Author Contributions

<sup>†</sup>D.P. and N.S. contributed equally to this work.

##### Notes

The authors declare no competing financial interest.

#### ■ ACKNOWLEDGMENTS

N.S., D.P., and L.D.A.S. acknowledge Dr. Peter Elliott and Dr. Sangeeta Sharma for a stimulating and fruitful discussion about TDDFT calculations. This research received funding from the



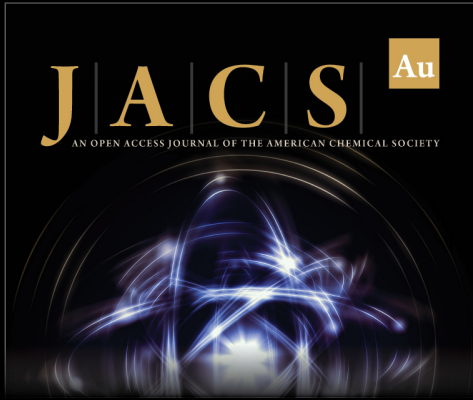
Netherlands Organization for Scientific Research (NWO) in the framework of the Materials for Sustainability and the Ministry of Economic Affairs in the framework of the PPP allowance and is also part of the NWO research program TOP-ECHO with project number 715.016.002 as well as the NWO Gravitation program "Research Centre for Integrated Nanophotonics". This work was carried out on the Dutch National e-Infrastructure with the support of SURF Cooperative.

## REFERENCES

- (1) Manzeli, S.; Ovchinnikov, D.; Pasquier, D.; Yazyev, O. V.; Kis, A. 2D Transition Metal Dichalcogenides. *Nat. Rev. Mater.* **2017**, *2*, No. 17033.
- (2) Xia, J.; Huang, X.; Liu, L.-Z.; Wang, M.; Wang, L.; Huang, B.; Zhu, D.-D.; Li, J.-J.; Gu, C.-Z.; Meng, X.-M. CVD Synthesis of Large-Area, Highly Crystalline MoSe<sub>2</sub> Atomic Layers on Diverse Substrates and Application to Photodetectors. *Nanoscale* **2014**, *6*, 8949–8955.
- (3) Late, D. J.; Huang, Y.-K.; Liu, B.; Acharya, J.; Shirodkar, S. N.; Luo, J.; Yan, A.; Charles, D.; Waghmare, U. V.; Dravid, V. P.; Rao, C. N. R. Sensing Behavior of Atomically Thin-Layered MoS<sub>2</sub> Transistors. *ACS Nano* **2013**, *7*, 4879–4891.
- (4) Donarelli, M.; Prezioso, S.; Perrozzi, F.; Bisti, F.; Nardone, M.; Giancaterini, L.; Cantalini, C.; Ottaviano, L. Response to NO<sub>2</sub> and Other Gases of Resistive Chemically Exfoliated MoS<sub>2</sub>-Based Gas Sensors. *Sens. Actuators, B* **2015**, *207*, 602–613.
- (5) Feng, J.; Qian, X.; Huang, C.-W.; Li, J. Strain-Engineered Artificial Atom as a Broad-Spectrum Solar Energy Funnel. *Nat. Photonics* **2012**, *6*, 866–872.
- (6) Pospischil, A.; Furchi, M. M.; Mueller, T. Solar-Energy Conversion and Light Emission in an Atomic Monolayer p–n Diode. *Nat. Nanotechnol.* **2014**, *9*, 257–261.
- (7) Mueller, T.; Malic, E. Exciton Physics and Device Application of Two-Dimensional Transition Metal Dichalcogenide Semiconductors. *npj 2D Mater. Appl.* **2018**, *2*, No. 29.
- (8) Wilson, J. A.; Yoffe, A. D. The Transition Metal Dichalcogenides Discussion and Interpretation of the Observed Optical, Electrical and Structural Properties. *Adv. Phys.* **1969**, *18*, 193–335.
- (9) Wang, Q. H.; Kalantar-Zadeh, K.; Kis, A.; Coleman, J. N.; Strano, M. S. Electronics and Optoelectronics of Two-Dimensional Transition Metal Dichalcogenides. *Nat. Nanotechnol.* **2012**, *7*, 699–712.
- (10) Splendiani, A.; Sun, L.; Zhang, Y.; Li, T.; Kim, J.; Chim, C.-Y.; Galli, G.; Wang, F. Emerging Photoluminescence in Monolayer MoS<sub>2</sub>. *Nano Lett.* **2010**, *10*, 1271–1275.
- (11) Mak, K. F.; He, K.; Shan, J.; Heinz, T. F. Control of Valley Polarization in Monolayer MoS<sub>2</sub> by Optical Helicity. *Nat. Nanotechnol.* **2012**, *7*, 494–498.
- (12) Chernikov, A.; Berkelbach, T. C.; Hill, H. M.; Rigosi, A.; Li, Y.; Aslan, O. B.; Reichman, D. R.; Hybertsen, M. S.; Heinz, T. F. Exciton Binding Energy and Nonhydrogenic Rydberg Series in Monolayer WS<sub>2</sub>. *Phys. Rev. Lett.* **2014**, *113*, No. 076802.
- (13) Song, J.-G.; Ryu, G. H.; Lee, S. J.; Sim, S.; Lee, C. W.; Choi, T.; Jung, H.; Kim, Y.; Lee, Z.; Myoung, J.-M.; et al. Controllable Synthesis of Molybdenum Tungsten Disulfide Alloy for Vertically Composition-Controlled Multilayer. *Nat. Commun.* **2015**, *6*, No. 7817.
- (14) Chen, Y.; Xi, J.; Dumcenco, D. O.; Liu, Z.; Suenaga, K.; Wang, D.; Shuai, Z.; Huang, Y.-S.; Xie, L. Tunable Band Gap Photoluminescence from Atomically Thin Transition-Metal Dichalcogenide Alloys. *ACS Nano* **2013**, *7*, 4610–4616.
- (15) Dumcenco, D. O.; Kobayashi, H.; Liu, Z.; Huang, Y.-S.; Suenaga, K. Visualization and Quantification of Transition Metal Atomic Mixing in Mo<sub>1-x</sub>W<sub>x</sub>S<sub>2</sub> Single Layers. *Nat. Commun.* **2013**, *4*, No. 1351.
- (16) Liu, H.; Antwi, K. K. A.; Chua, S.; Chi, D. Vapor-Phase Growth and Characterization of Mo<sub>1-x</sub>W<sub>x</sub>S<sub>2</sub> (0 ≤ x ≤ 1) Atomic Layers on 2-Inch Sapphire Substrates. *Nanoscale* **2014**, *6*, 624–629.
- (17) Rigosi, A. F.; Hill, H. M.; Rim, K. T.; Flynn, G. W.; Heinz, T. F. Electronic Band Gaps and Exciton Binding Energies in Monolayer Mo<sub>x</sub>W<sub>1-x</sub>S<sub>2</sub> Transition Metal Dichalcogenide Alloys Probed by Scanning Tunneling and Optical Spectroscopy. *Phys. Rev. B* **2016**, *94*, No. 075440.
- (18) Gao, Y.; Liu, J.; Zhang, X.; Lu, G. Unraveling Structural and Optical Properties of Two-Dimensional Mo<sub>x</sub>W<sub>1-x</sub>S<sub>2</sub> Alloys. *J. Phys. Chem. C* **2021**, *125*, 774–781.
- (19) Xi, J.; Zhao, T.; Wang, D.; Shuai, Z. Tunable Electronic Properties of Two-Dimensional Transition Metal Dichalcogenide Alloys: A First-Principles Prediction. *J. Phys. Chem. Lett.* **2014**, *5*, 285–291.
- (20) Kaasbjerg, K.; Thygesen, K. S.; Jacobsen, K. W. Phonon-Limited Mobility in n-Type Single-Layer MoS<sub>2</sub> from First Principles. *Phys. Rev. B* **2012**, *85*, No. 115317.
- (21) Zhao, W.; Ribeiro, R. M.; Toh, M.; Carvalho, A.; Kloc, C.; Neto, A. H. C.; Eda, G. Origin of Indirect Optical Transitions in Few-Layer MoS<sub>2</sub>, WS<sub>2</sub>, and WSe<sub>2</sub>. *Nano Lett.* **2013**, *13*, 5627–5634.
- (22) Ruppert, C.; Chernikov, A.; Hill, H. M.; Rigosi, A. F.; Heinz, T. F. The Role of Electronic and Phononic Excitation in the Optical Response of Monolayer WS<sub>2</sub> after Ultrafast Excitation. *Nano Lett.* **2017**, *17*, 644–651.
- (23) Raja, A.; Selig, M.; Berghäuser, G.; Yu, J.; Hill, H. M.; Rigosi, A. F.; Brus, L. E.; Knorr, A.; Heinz, T. F.; Malic, E.; Chernikov, A. Enhancement of Exciton–Phonon Scattering from Monolayer to Bilayer WS<sub>2</sub>. *Nano Lett.* **2018**, *18*, 6135–6143.
- (24) Selig, M.; Berghäuser, G.; Raja, A.; Nagler, P.; Schüller, C.; Heinz, T. F.; Korn, T.; Chernikov, A.; Malic, E.; Knorr, A. Excitonic Linewidth and Coherence Lifetime in Monolayer Transition Metal Dichalcogenides. *Nat. Commun.* **2016**, *7*, No. 13279.
- (25) Christiansen, D.; Selig, M.; Berghäuser, G.; Schmidt, R.; Niehues, I.; Schneider, R.; Arora, A.; de Vasconcellos, S. M.; Bratschkitsch, R.; Malic, E.; et al. Phonon Sidebands in Monolayer Transition Metal Dichalcogenides. *Phys. Rev. Lett.* **2017**, *119*, No. 187402.
- (26) Helmrich, S.; Schneider, R.; Achtstein, A. W.; Arora, A.; Herzog, B.; de Vasconcellos, S. M.; Kolarczik, M.; Schöps, O.; Bratschkitsch, R.; Woggon, U.; et al. Exciton–Phonon Coupling in Mono- and Bilayer MoTe<sub>2</sub>. *2D Mater.* **2018**, *5*, No. 045007.
- (27) Ho, C. H.; Wu, C. S.; Huang, Y. S.; Liao, P. C.; Tiong, K. K. Temperature Dependence of Energies and Broadening Parameters of the Band-Edge Excitons of Single Crystals. *J. Phys.: Condens. Matter* **1998**, *10*, 9317–9328.
- (28) Schulpen, J. J. P. M.; Verheijen, M. A.; Kessels, W. M. M.; Vandalon, V.; Bol, A. A. Controlling Transition Metal Atomic Ordering in Two-Dimensional Mo<sub>1-x</sub>W<sub>x</sub>S<sub>2</sub> Alloys. *ArXiv211106289 Cond-Mat* 2021.
- (29) Dewhurst, K.; Sharma, S.; Nordstrom, L.; Cricchio, F.; Bultmark, F.; Gross, H. Introduction To The Elk Code. [www.elk.sourceforge.io](http://www.elk.sourceforge.io).
- (30) Perdew, J. P.; Burke, K.; Ernzerhof, M. Generalized Gradient Approximation Made Simple. *Phys. Rev. Lett.* **1996**, *77*, No. 3865.
- (31) Petkov, V.; Billinge, S. J. L.; Larson, P.; Mahanti, S. D.; Vogt, T.; Rangan, K. K.; Kanatzidis, M. G. Structure of Nanocrystalline Materials Using Atomic Pair Distribution Function Analysis: Study of LiMoS<sub>2</sub>. *Phys. Rev. B* **2002**, *65*, No. 092105.
- (32) Schutte, W. J.; De Boer, J. L.; Jellinek, F. Crystal Structures of Tungsten Disulfide and Diselenide. *J. Solid State Chem.* **1987**, *70*, 207–209.
- (33) Sharma, S.; Dewhurst, J. K.; Gross, E. K. U. Optical Response of Extended Systems Using Time-Dependent Density Functional Theory. In *Topics in Current Chemistry*; Springer Berlin Heidelberg, 2014; Vol. 347, pp 235–257.
- (34) Wooten, F. *Optical Properties of Solids*; Academic Press: Davis, California, 2013.
- (35) Sharma, S.; Dewhurst, J. K.; Sanna, A.; Gross, E. K. U. Bootstrap Approximation for the Exchange-Correlation Kernel of Time-Dependent Density-Functional Theory. *Phys. Rev. Lett.* **2011**, *107*, No. 186401.





- (36) Zhao, W.; Ghorannevis, Z.; Amara, K. K.; Pang, J. R.; Toh, M.; Zhang, X.; Kloc, C.; Tan, P. H.; Eda, G. Lattice Dynamics in Mono- and Few-Layer Sheets of  $\text{WS}_2$  and  $\text{WSe}_2$ . *Nanoscale* **2013**, *5*, 9677–9683.
- (37) Latzke, D. W.; Zhang, W.; Suslu, A.; Chang, T.-R.; Lin, H.; Jeng, H.-T.; Tongay, S.; Wu, J.; Bansil, A.; Lanzara, A. Electronic Structure, Spin-Orbit Coupling, and Interlayer Interaction in Bulk  $\text{MoS}_2$  and  $\text{WS}_2$ . *Phys. Rev. B* **2015**, *91*, No. 235202.
- (38) Fan, X.; Singh, D. J.; Zheng, W. Valence Band Splitting on Multilayer  $\text{MoS}_2$ : Mixing of Spin-Orbit Coupling and Interlayer Coupling. *J. Phys. Chem. Lett.* **2016**, *7*, 2175–2181.
- (39) Palumbo, M.; Bernardi, M.; Grossman, J. C. Exciton Radiative Lifetimes in Two-Dimensional Transition Metal Dichalcogenides. *Nano Lett.* **2015**, *15*, 2794–2800.
- (40) Qiu, D. Y.; da Jornada, F. H.; Louie, S. G. Optical Spectrum of  $\text{MoS}_2$ : Many-Body Effects and Diversity of Exciton States. *Phys. Rev. Lett.* **2013**, *111*, No. 216805.
- (41) Kunstmann, J.; Wendumu, T. B.; Seifert, G. Localized Defect States in  $\text{MoS}_2$  Monolayers: Electronic and Optical Properties. *Phys. Status Solidi B* **2017**, *254*, No. 1600645.
- (42) Yu, P. Y.; Cardona, M. *Fundamentals of Semiconductors: Physics and Materials Properties*, 4th ed.; Graduate Texts in Physics; Springer-Verlag: Berlin Heidelberg, 2010.
- (43) King-Smith, R. D.; Needs, R. J.; Heine, V.; Hodgson, M. J. A First-Principle Calculation of the Temperature Dependence of the Indirect Band Gap of Silicon. *Europhys. Lett. EPL* **1989**, *10*, 569–574.
- (44) Huang, J.; Hoang, T. B.; Mikkelsen, M. H. Probing the Origin of Excitonic States in Monolayer  $\text{WSe}_2$ . *Sci. Rep.* **2016**, *6*, No. 22414.
- (45) Christopher, J. W.; Goldberg, B. B.; Swan, A. K. Long Tailed Trions in Monolayer  $\text{MoS}_2$ : Temperature Dependent Asymmetry and Resulting Red-Shift of Trion Photoluminescence Spectra. *Sci. Rep.* **2017**, *7*, No. 14062.
- (46) He, Z.; Sheng, Y.; Rong, Y.; Lee, G.-D.; Li, J.; Warner, J. H. Layer-Dependent Modulation of Tungsten Disulfide Photoluminescence by Lateral Electric Fields. *ACS Nano* **2015**, *9*, 2740–2748.
- (47) O'Donnell, K. P.; Chen, X. Temperature Dependence of Semiconductor Band Gaps. *Appl. Phys. Lett.* **1991**, *58*, 2924–2926.
- (48) Wang, Z.-W.; Li, R.-Z.; Dong, X.-Y.; Xiao, Y.; Li, Z.-Q. Temperature Dependence of the Excitonic Spectra of Monolayer Transition Metal Dichalcogenides. *Front. Phys.* **2018**, *13*, No. 137305.
- (49) Gaur, A. P. S.; Sahoo, S.; Scott, J. F.; Katiyar, R. S. Electron-Phonon Interaction and Double-Resonance Raman Studies in Monolayer  $\text{WS}_2$ . *J. Phys. Chem. C* **2015**, *119*, 5146–5151.
- (50) Dey, P.; Paul, J.; Wang, Z.; Stevens, C. E.; Liu, C.; Romero, A. H.; Shan, J.; Hilton, D. J.; Karaickaj, D. Optical Coherence in Atomic-Monolayer Transition-Metal Dichalcogenides Limited by Electron-Phonon Interactions. *Phys. Rev. Lett.* **2016**, *116*, No. 127402.
- (51) Rudin, S.; Reinecke, T. L.; Segall, B. Temperature-Dependent Exciton Linewidths in Semiconductors. *Phys. Rev. B* **1990**, *42*, No. 11218.
- (52) Evans, B. L.; Young, P. A. Optical Absorption and Dispersion in Molybdenum Disulphide. *Proc. R. Soc. London, Ser. A* **1965**, *284*, 402–422.
- (53) McCreary, K. M.; Hanbicki, A. T.; Sivaram, S. V.; Jonker, B. T. A- and B-Exciton Photoluminescence Intensity Ratio as a Measure of Sample Quality for Transition Metal Dichalcogenide Monolayers. *APL Mater.* **2018**, *6*, No. 111106.
- (54) Tongay, S.; Zhou, J.; Ataca, C.; Lo, K.; Matthews, T. S.; Li, J.; Grossman, J. C.; Wu, J. Thermally Driven Crossover from Indirect toward Direct Bandgap in 2D Semiconductors:  $\text{MoSe}_2$  versus  $\text{MoS}_2$ . *Nano Lett.* **2012**, *12*, 5576–5580.
- (55) Arora, A.; Koperski, M.; Nogajewski, K.; Marcus, J.; Faugeras, C.; Potemski, M. Excitonic Resonances in Thin Films of  $\text{WSe}_2$ : From Monolayer to Bulk Material. *Nanoscale* **2015**, *7*, 10421–10429.
- (56) Arora, A.; Nogajewski, K.; Molas, M.; Koperski, M.; Potemski, M. Exciton Band Structure in Layered  $\text{MoSe}_2$ : From a Monolayer to the Bulk Limit. *Nanoscale* **2015**, *7*, 20769–20775.
- (57) Mattinen, M.; Leskelä, M.; Ritala, M. Atomic Layer Deposition of 2D Metal Dichalcogenides for Electronics, Catalysis, Energy Storage, and Beyond. *Adv. Mater. Interfaces* **2021**, *8*, No. 2001677.
- (58) Martin, R. M.; Reining, L.; Ceperley, D. M. *Interacting Electrons: Theory and Computational Approaches*; Cambridge University Press: Cambridge, 2016.



**JACS** Au  
AN OPEN ACCESS JOURNAL OF THE AMERICAN CHEMICAL SOCIETY

Editor-in-Chief  
**Prof. Christopher W. Jones**  
Georgia Institute of Technology, USA

**Open for Submissions** 

pubs.acs.org/jacsau  ACS Publications  
Most Trusted. Most Cited. Most Read.